International Journal of Solids and Structures 50 (2013) 3254–3265

Contents lists available at SciVerse ScienceDirect

International Journal of Solids and Structures

journal homepage: www.elsevier.com/locate/ijsolstr

Temperature analysis of one-dimensional NiTi shape memory alloys under different loading rates and boundary conditions

S.Y. Yang, G.S. Dui *

Institute of Engineering Mechanics, Beijing Jiaotong University, Beijing 100044, PR China

ARTICLE INFO

Article history:
Received 19 June 2012
Received in revised form 24 April 2013
Available online 13 June 2013

Keywords:
Shape memory alloys
Loading rates
Boundary conditions
Temperature variation

ABSTRACT

Superelastic polycrystalline NiTi shape memory alloys under tensile loading accompany the strain localization and propagation phenomena. Experiments showed that the number of moving phase fronts and the mechanical behavior are very sensitive to the loading rate due to the release/absorption of latent heat and the material's inherent temperature sensitivity of the transformation stress. In this paper, the moving heat source method based on the heat diffusion equation is used to study the temperature evolution of one-dimensional superelastic NiTi specimen under different loading rates and boundary conditions with moving heat sources or a uniform heat source. Comparisons of temperature variations with different boundary conditions show that the heat exchange at the boundaries plays a major role in the nonuniform temperature profile that directly relates to the localized deformation. Analytical relation between the front temperature of a single phase front, the inherent Clausius–Clapeyron relation (sensitivity of the material's transformation stress with temperature), heat transfer boundary conditions and the loading rate is established to analyze the nucleation of new phase fronts. Finally, the rate-dependent stress hysteresis is also simply discussed by using the results of temperature analyses.

1. Introduction

Shape memory alloys (SMAs) have been widely used in many practical engineering branches due to their unique shape memory effect and pseudo-elasticity. The pseudo-elastic response, especially refers to the fact that, relative large strains (up to 8%) can be imposed by mechanical loading and then recover via a hysteresis loop upon unloading. This phenomenon arises from a reversible stress-induced martensitic transformation between two different crystalline phases, austenite (low strain phase) and detwinned martensite (high strain phase) (Abeyaratne and Knowles, 1993; Otsuka and Wayman, 1998; Bhattacharya, 2003). In recent years, it was observed in many experiments (Brinson et al., 2004; Puglisi and Truskinovsky, 2005; Sun and He, 2008) that there are non-continuous nucleation and growth of micro-domains at the grain-size level in the process of stress-induced phase transformation in polycrystalline, accompanying intrinsic material instability and dissipative evolution of these domains. For fine-grained polycrystalline NiTi under tensile loading, these micro-domains can collectively form macroscopic domains. Detailed experiments (Leo et al., 1993; Shaw and Kyriakides, 1995, 1997; Sun and Li, 2002; Feng and Sun, 2006; Grabe and Bruhns, 2008; He et al., 2010; Zhang et al., 2010) also showed that polycrystalline NiTi SMAs under stretching deform via the nucleation and growth of macroscopic martensite domains which consist of almost fully-transformed grains. The transformation is accompanied by unstable mechanical behavior and localized deformation (the existence of domains and phase fronts). In fact, phase fronts are propagating necks separating low strain regions from high strain regions and can be observed by the naked eye as slight glints along the specimen axial direction.

During a pseudo-elastic transformation, a large amount of heat can be generated due to phase change, resulting in temperature variations that readily impact the behavior of SMAs. With high applied loading rate, the resulting high heat rate causes a swift temperature variation of the material. This leads to the significant variation in the stress–strain response due to the temperature sensitivity of the transformation stress of NiTi SMAs (Leo et al., 1993; Shaw and Kyriakides, 1995, 1997; Tobushi et al., 1998; Grabe and Bruhns, 2008; He et al., 2010; Zhang et al., 2010). These rate-dependent mechanical behaviors could be a major concern in the design and application of SMA devices, especially the performance, reliability, and controllability of the material as passive or active constituents. From experimental point of view, the dependence on loading rates is stronger in air than in water, and experimental results suggested that this dependence is mainly a temperature effect rather than a usual visco-elastic effect (Shaw and Kyriakides, 1995). Grabe and Bruhns (2008) confirmed this conclusion by showing that this dependence disappears if the temperature of the specimen is kept constant.

* Corresponding author. Tel.: +86 1051688437; fax: +86 1051682094.
E-mail address: gsdui@center.njtu.edu.cn (G.S. Dui).

0020-7683/$ - see front matter © 2013 Elsevier Ltd. All rights reserved.
http://dx.doi.org/10.1016/j.ijsolstr.2013.05.026

Nomenclature

x, m	axial coordinate and moving heat source position (m)
t, τ	time and integration time variable (s)
T, T_0	axial temperature of specimen and ambient temperature (°C)
θ	axial temperature difference between T and T_0 (°C)
L, r	length and radius of specimen (m)
P, L_c	perimeter and characteristic lateral length of specimen (m)
A	cross-sectional area of specimen (m^2)
C_V	heat capacity per unit volume (J/(m^3 K))
k	thermal conductivity (W/(m K))
h	heat convection coefficient (air) (W/(m^2 K))
Bi	Biot number
b_{int}	rate of internal heat source per unit volume (W/m^3)
i	index of summation, $i = 1,2,3,\ldots,\infty$
Δt, t_i	time interval and an indexed time representing each successive term in the series (s)
$\Delta Q(t_i)$	transient heat source at time t_i (J)
$\theta_i(x,t\|t_i)$	axial temperature variation caused by $\Delta Q(t_i)$ (^{0}C)
$\theta_{M1},\theta_{M2},\theta_U$	initial temperature variation caused by $\Delta Q(t_i)$ at time t_i (°C)
q	release rate of latent heat source (J/s)
l	released latent heat per unit volume (J/m^3)
$\dot{\delta}$, v_N	elongation rate and speed of moving phase front (m/s)
N	number of moving phase fronts
$\sigma_N,\sigma_P,\Delta\sigma$	nucleation, propagation and isothermal dropped stresses (MPa)
$\varepsilon,\varepsilon_T$	engineering axial strain and transformation strain
t_T	transformation time (s)
θ_0	adiabatic temperature rise (°C)
θ_{front}	phase front temperature variation (°C)
[x]	non-dimensional axial coordinate
[m]	non-dimensional moving heat source position
[t]	non-dimensional time
$[\theta]$	non-dimensional temperature variation
$[\theta_f]$	non-dimensional phase front temperature variation

According to the classical Clausius–Clapeyron relation specialized to uniaxial stress, the forward (Austenite to Martensite) and reverse (Martensite to Austenite) transformation stresses of NiTi SMAs can be well approximated as linear functions of temperature (Shaw and Kyriakides, 1995, 1997; Churchill et al., 2009; Sun et al., 2012). Therefore, the analysis of the specimen's temperature is useful for studying the rate-dependent stress–strain curve. However, the problem is that moving phase fronts and boundary conditions make temperature fields macroscopically nonuniform in the specimen.

Some previous works studied the rate-dependent phenomena of NiTi SMAs (Bruno et al., 1995; Shaw, 2000; Auricchio and Sacco, 2001; Iadicola and Shaw, 2004; Vitiello et al., 2005; Chang et al., 2006; Zhu and Zhang, 2007; He and Sun, 2010, 2011; Morin et al., 2011; Grandi et al., 2012) and other SMAs like CuZnAl (Entemeyer et al., 2000; Balandraud et al., 2001; Chrysochoos et al., 2003). Bruno et al. (1995) presented a related continuous free boundary model and used its asymptotics to derive a closed-form expression that relates the rate-dependent experimental observables, especially the dependence of the widths of the hysteresis loops on the elongation rate. The asymptotic calculations provided predictions which were in close agreement with numerical values obtained by integration of the Eqs. (1)–(4) in Bruno et al. (1995) and experimental results for a wide range of experimental parameters (Leo et al., 1993). In fact, the closed-form expression of temperature profiles caused by moving phase front is only exact in the limit of an infinitely long wire. If the specimen is long (for example, 13 cm and 78 cm NiTi wire (Leo et al., 1993)), the differences between predictions and experimental data are negligible. And the closed-form expression is accurate enough to analyze the axial temperature variation in one-dimensional specimen. However, many experimental specimens are only a few millimeters long (like 17 mm gauge length of NiTi sheet (He et al., 2010) or 24 mm length of wire-like monocrystalline CuZnAl (Balandraud et al., 2001)). In these scenarios the closed-form expression has its own limitation to analyze the temperature variation of short specimen. Furthermore, the insulated attachments at the ends of the wire used in Bruno et al. (1995) should also be carefully treated in the case of short specimen. Iadicola and Shaw (2004) studied the temperature evolution of a thin NiTi wire with moving point heat sources as well as a uniform heat source in order to investigate the trends of localized nucleation and propagation phenomena for a wide range of loading rates and ambient thermal conditions. Unlike the insulated attachments, they made assumptions that wire is held at a fixed temperature at the ends and the grips of the test machine are thermally conductive and massive enough to act as thermal heat sinks. Chrysochoos et al. (2003) modeled the thermo-mechanical couplings accompanying the phase transformation in single-crystal CuZnAl samples and showed that the amazing mechanical effects observed and modeled (for example, the "creep" and "anti-creep" phenomena) are the consequences of the time-dependency through heat diffusion. In their model, the convective boundary condition was used to define the heat exchange between the specimen ends and ambient conditions. Since different boundary conditions result in different temperature fields that directly relates to the rate-dependent mechanical responses of SMAs, the effects of boundary conditions should be carefully analyzed.

In this paper we analyze the temperature fields in one-dimensional superelastic NiTi SMAs under different loading rates and boundary conditions during the forward transformation. The results provide useful information about the thermo-mechanical couplings related to localized nucleation events and the propagation of phase fronts. Moreover, the thermal analyses are very useful to understand the sensitivity of the thermal behavior to the transformation kinetics. The remaining parts of this paper are organized as follows. In Section 2, we discuss the heat equation, different internal heat sources and thermal boundary conditions. The moving heat source method is used to obtain the temperature variations caused by moving heat sources or a uniform heat source. In Section 3, numerical simulations of the axial temperature evolution of a thin NiTi SMA wire during the forward phase transformation with three different boundary conditions are given. Comparisons of these temperature variations clearly show the effects of boundary conditions on the temperature variation. Section 4 discusses the nucleation of new phase fronts and the rate-dependent stress hysteresis basing on the temperature dependence of the transformation stress and the above temperature analyses. The closed-form expression is a special case of Eq. (7) in this paper. Conclusions are given in Section 5.

2. Theoretical analysis

In this paper, only the axial temperature field of one-dimensional SMAs is discussed. Because of the excellent heat conduction

Table 1
Results of temperature variations.

Type	Results
$\langle S\rangle+\langle I\rangle+\langle G\rangle$	$\frac{2lv_1}{LC_V}\sum_{n=1}^{\infty}\sin(\frac{n\pi v_1\tau}{L})\sin(\frac{n\pi x}{L})e^{-B_n(t-\tau)}$
$\langle S\rangle+\langle I\rangle+\langle\theta\rangle$	$\frac{2lv_1}{LC_V}\sum_{n=1}^{\infty}\sin(\frac{n\pi x}{L})e^{-B_nt}P_n$
$\langle S\rangle+\langle II\rangle+\langle G\rangle$	$\frac{2lv_1}{LC_V}\left[\frac{1}{2}e^{-D(t-\tau)}+\sum_{n=1}^{\infty}\cos(\frac{n\pi v_1\tau}{L})\cos(\frac{n\pi x}{L})e^{-B_n(t-\tau)}\right]$
$\langle S\rangle+\langle II\rangle+\langle\theta\rangle$	$\frac{2lv_1}{LC_V}\left[\frac{(1-e^{-Dt})}{2D}+\sum_{n=1}^{\infty}\cos(\frac{n\pi x}{L})e^{-B_nt}Q_n\right]$
$\langle S\rangle+\langle III\rangle+\langle G\rangle$	$\frac{lv_1}{\sqrt{4\pi kC_V(t-\tau)}}e^{-\left[D(t-\tau)+\frac{(x-v_1\tau)^2}{4k(t-\tau)/C_V}\right]}$
$\langle S\rangle+\langle III\rangle+\langle\theta\rangle$	$\frac{lv_1}{\sqrt{4\pi kC_V}}\int_0^t\frac{1}{\sqrt{(t-\tau)}}e^{-\left[D(t-\tau)+\frac{(x-v_1\tau)^2}{4k(t-\tau)/C_V}\right]}d\tau$
$\langle T\rangle+\langle I\rangle+\langle G\rangle$	$\frac{2lv_2}{LC_V}\sum_{n=1}^{\infty}\{\sin(\frac{n\pi v_2\tau}{L})+\sin\left[\frac{n\pi}{L}(L-v_2\tau)\right]\}\sin(\frac{n\pi x}{L})e^{-B_n(t-\tau)}$
$\langle T\rangle+\langle I\rangle+\langle\theta\rangle$	$\frac{2lv_2}{LC_V}\sum_{n=1}^{\infty}\sin(\frac{n\pi x}{L})e^{-B_nt}R_n$
$\langle T\rangle+\langle II\rangle+\langle G\rangle$	$\frac{2lv_2}{LC_V}\{e^{-D(t-\tau)}+\sum_{n=1}^{\infty}\left[\cos(\frac{n\pi v_2\tau}{L})+\cos\left[\frac{n\pi}{L}(L-v_2\tau)\right]\right]\cos(\frac{n\pi x}{L})e^{-B_n(t-\tau)}\}$
$\langle T\rangle+\langle II\rangle+\langle\theta\rangle$	$\frac{2lv_2}{LC_V}\left[\frac{(1-e^{-Dt})}{D}+\sum_{n=1}^{\infty}\cos(\frac{n\pi x}{L})e^{-B_nt}S_n\right]$
$\langle T\rangle+\langle III\rangle+\langle G\rangle$	$\frac{lv_2}{\sqrt{4\pi kC_V(t-\tau)}}e^{-D(t-\tau)}\left[e^{-\frac{(x-v_2\tau)^2}{4k(t-\tau)/C_V}}+e^{-\frac{(x-L+v_2\tau)^2}{4k(t-\tau)/C_V}}\right]$
$\langle T\rangle+\langle III\rangle+\langle\theta\rangle$	$\frac{lv_2}{\sqrt{4\pi kC_V}}\int_0^t\frac{1}{\sqrt{(t-\tau)}}e^{-D(t-\tau)}\left[e^{-\frac{(x-v_2\tau)^2}{4k(t-\tau)/C_V}}+e^{-\frac{(x-L+v_2\tau)^2}{4k(t-\tau)/C_V}}\right]d\tau$
$\langle U\rangle+\langle I\rangle+\langle G\rangle$	$\frac{2l\delta}{LC_V\varepsilon_T}\sum_{n=1}^{\infty}\frac{[1-(-1)^n]}{n\pi}\sin(\frac{n\pi x}{L})e^{-B_n(t-\tau)}$
$\langle U\rangle+\langle I\rangle+\langle\theta\rangle$	$\frac{2l\delta}{LC_V\varepsilon_T}\sum_{n=1}^{\infty}\frac{[1-(-1)^n]}{n\pi}\frac{(1-e^{-B_nt})}{B_n}\sin(\frac{n\pi x}{L})$
$\langle U\rangle+\langle II\rangle+\langle G\rangle$	$\frac{l\delta}{LC_V\varepsilon_T}e^{-D(t-\tau)}$
$\langle U\rangle+\langle II\rangle+\langle\theta\rangle$	$\frac{l\delta}{LC_V\varepsilon_TD}(1-e^{-Dt})$
$\langle U\rangle+\langle III\rangle+\langle G\rangle$	$\frac{l\delta}{L\varepsilon_T\sqrt{4\pi kC_V(t-\tau)}}\int_0^L e^{-\left[D(t-\tau)+\frac{(x-\xi)^2}{4k(t-\tau)/C_V}\right]}d\xi$
$\langle U\rangle+\langle III\rangle+\langle\theta\rangle$	$\frac{l\delta}{L\varepsilon_T\sqrt{4\pi kC_V}}\int_0^t\int_0^L\frac{1}{\sqrt{(t-\tau)}}e^{-\left[D(t-\tau)+\frac{(x-\xi)^2}{4k(t-\tau)/C_V}\right]}d\xi d\tau$

$v_1=\frac{\delta}{\varepsilon_T}$, $v_2=\frac{\delta}{2\varepsilon_T}$, $D=\frac{hP}{AC_V}$, $A_n=\begin{cases}\frac{n\pi v_1}{L} & N=1\\ \frac{n\pi v_2}{L} & N=2\end{cases}$, $B_n=\frac{hP}{AC_V}+\frac{n^2\pi^2}{L^2}\frac{k}{C_V}$, $P_n=\frac{A_n+e^{B_nt}(B_n\sin A_nt-A_n\cos A_nt)}{A_n^2+B_n^2}$, $Q_n=\frac{-B_n+e^{B_nt}(B_n\cos A_nt+A_n\sin A_nt)}{A_n^2+B_n^2}$, $R_n=[1-(-1)^n]P_n$ and $S_n=[1+(-1)^n]Q_n$. $\langle S\rangle$, $\langle T\rangle$, $\langle U\rangle$ represent the case of single moving heat source, two moving heat sources, and uniform heat source, respectively. $\langle I\rangle$, $\langle II\rangle$, $\langle III\rangle$ represent the first, second, and 'third' boundary condition, respectively. $\langle G\rangle$, $\langle\theta\rangle$ are $G(x,t|\tau)$ and $\theta(x,t)$, respectively. $\langle S\rangle+\langle I\rangle+\langle\theta\rangle$ represents temperature variation $\theta(x,t)$ caused by a single moving heat source $\langle S\rangle$ with the first boundary condition $\langle I\rangle$.

and small effective radius of NiTi specimen that leads to a very small Biot number, the cross-sectional temperature can be approximated to be uniform. (Biot number: the ratio of the radial thermal conduction resistance to the lateral boundary thermal resistance, $Bi = L_ch/k \ll 0.1$, where L_c, h and k are, respectively, the characteristic length, i.e., ratio of cross-sectional area A to perimeter P, the heat convection coefficient and the thermal conductivity. Using the material constants in Table 2, the NiTi SMA wire only has a Biot number of 5.3×10^{-5} in air.)

Based on the above simplification, the heat equation can be written as

$$C_V\frac{\partial\theta(x,t)}{\partial t}-k\frac{\partial^2\theta(x,t)}{\partial x^2}+\frac{hP}{A}\theta(x,t)=b_{\text{int}} \tag{1}$$

where $\theta = T(x,t)-T_0$ is the axial temperature difference between the specimen temperature T and the ambient temperature T_0, C_V is the heat capacity per unit volume, k is the thermal conductivity, h is the heat convection coefficient, P is the cross-sectional perimeter, A is the cross-sectional area, and b_{int} is the rate of internal heat source per unit volume. To simplify the discussion, P and A are assumed to be constant in the axial direction and the material constants C_V, k and h are assumed the same in martensite and austenite.

Generally speaking, the value of heat source b_{int} produced by the material is often divided into two terms H_{tmc} and D_{mec} (Leclercq and Lexcellent, 1996; Entemeyer et al., 2000; Auricchio and Sacco, 2001; Lim and McDowell, 2002; Favier et al., 2007): H_{tmc} represents the heat production associated to the thermomechanical coupling; D_{mec} represents the heat production associated to the mechanical dissipation, also named intrinsic dissipation, related to any mechanical irreversible phenomena. The heat source H_{tmc}, corresponding to the coupling between the temperature T and the other state variables like strain ε and martensite volume

Table 2
NiTi SMA wire material properties and geometry (Leo et al., 1993).

Property	Symbol	Value	Unit
Composition	50.5 Ni (at.%)		
Radius	r	0.326	mm
Perimeter	P	2.048	mm
Area	A	0.3339	mm^2
Length	L	130	mm
Thermal conductivity	k	20	W/(m K)
Heat convection coefficient (air)	h	6.5	W/(m^2 K)
Latent heat	l	43	MPa
Transformation strain	ε_T	0.068	
Heat capacity (300 K)	C_V	3.225×10^6	J/(m^3 K)

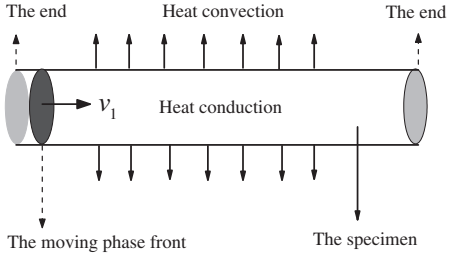

Fig. 1. Schematic diagram of a single moving phase front in one-dimentional NiTi wire.

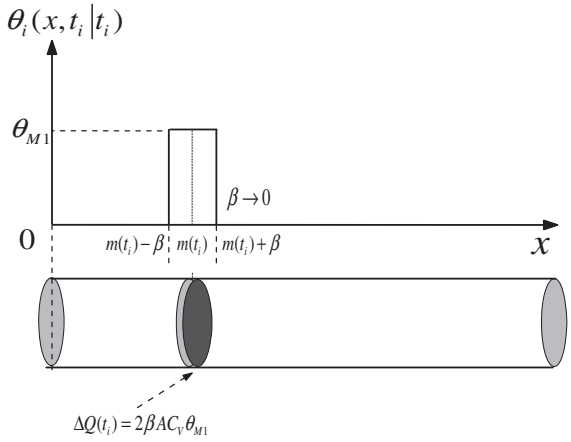

Fig. 2. Schematic diagram of a transient point heat source at position $m(t_i)$ and time t_i.

fraction λ in the expression of the free energy ψ, is at least two terms here: the thermoelastic coupling heat source $T\frac{\partial^2\psi}{\partial T\partial\varepsilon}\dot{\varepsilon}$ and the latent heat source $T\frac{\partial^2\psi}{\partial T\partial\lambda}\dot{\lambda}$ due to phase change. Compared with other internal heat sources, the latent heat source plays a major role in the temperature variation of SMAs (Entemeyer et al., 2000; Morin et al., 2011). For the purpose of simplicity and without losing the key features, this paper only analyzes the influence of latent heat source on thermo-mechanical responses of NiTi SMAs.

Three boundary conditions at the specimen ends are discussed in this paper:

(1) Boundary condition of the first kind. If large metallic grips are used in the experiment, it is reasonable to assume the temperature of specimen ends, $T(0,t)$ and $T(L,t)$, is fixed at the ambient temperature T_0, and model the grips as perfect heat sinks which are thermally conductive and massive enough (Shaw, 2000; Iadicola and Shaw, 2004; Chang et al., 2006). This boundary condition is Dirichlet condition and can be written as

$$\theta(0,t)=T(0,t)-T_0=0;\theta(L,t)=T(L,t)-T_0=0 \tag{2}$$

(2) Boundary condition of the second kind. Bruno et al. (1995) assumed the insulated attachment at the ends of the NiTi SMA wire and there was no heat flux between the specimen ends and ambient conditions (or test machine grips). This boundary condition, Neumann condition, is often used to model the thermomechanical behavior of one-dimensional SMAs (Vitiello et al., 2005; Zhu and Zhang, 2007; He and Sun, 2011) and can be written as

$$\frac{\partial\theta(0,t)}{\partial x}=\frac{\partial[T(0,t)-T_0]}{\partial x}=0;\frac{\partial\theta(L,t)}{\partial x}=\frac{\partial[T(L,t)-T_0]}{\partial x}=0 \tag{3}$$

(3) Boundary condition of the 'third' kind. Chrysochoos et al. (2003) used the classical Robin condition (the usual third boundary condition) to study the effects of the thermomechanical coupling on the propagation of a phase front in a CuZnAl SMA monocrystal. However, precise definition of the longitudinal heat exchange coefficient between the specimen ends and the grips is difficult, the 'third' boundary condition used in this paper is defined as following: it is assumed that the heat flux at both ends of one-dimensional SMAs can continue to transfer in two virtual semi-infinite long one-dimensional specimens in which conduction of heat between the sample and the surroundings only exist. Moreover, geometry and material parameters of the two virtual specimens are assumed to be constant in the axial direction and the same as the one-dimensional SMAs. What's more, heat exchange between the specimen and the test machine grips is neglected. Based on the above definition, the temperature profile with the 'third' boundary condition can be obtained by using the Fourier integral transform method in the infinite range $-\infty < x < \infty$.

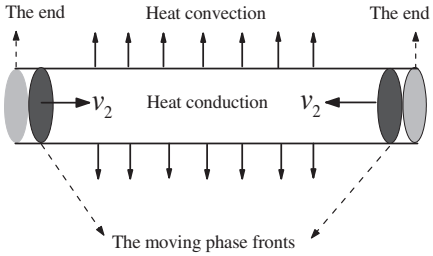

Fig. 3. Schematic diagram of two moving phase fronts in one-dimentional NiTi wire.

Using the moving heat source method, the axial temperature variation $\theta(x,t)=T(x,t)-T_0$ at time t caused by moving heat source in one-dimensional specimen is the sum of the response which would have been caused by each transient heat at different time and position in the time range $[0,t]$ individually. Dividing the time range $[0,t]$ into numerous small time interval $\Delta t=\frac{t}{\mathbf{M}}$, $\mathbf{M}\to\infty$ and discussing the transient time interval Δt at $t_i=\frac{i-1}{\mathbf{M}}t$, $i=1,2,3,\ldots,M$. The moving heat source moves to position $m=m(t_i)$ and releases heat $\Delta Q(t_i)=q(t_i)\Delta t$, where $q(t_i)$ is the release rate of the moving heat source. This $\Delta Q(t_i)$ can be seen as a transient heat at position $m=m(t_i)$ and time t_i, which causes the axial temperature variation $\theta_i(x,t|m(t_i),t_i)=\theta_i(x,t|t_i)=F(x,t|t_i)\Delta Q(t_i)=G(x,t|t_i)\Delta t$ at time $t>t_i$. Since the temperature variation $\theta(x,t)$ is the sum of each response, we finally have $\theta(x,t)=\lim_{\mathbf{M}\to\infty}\sum_{i=1}^{\mathbf{M}}\theta_i(x,t|t_i)=\lim_{\mathbf{M}\to\infty}\sum_{i=1}^{\mathbf{M}}G(x,t|t_i)\Delta t=\int_0^t G(x,t|\tau)d\tau$.

To obtain $\theta_i(x,t|t_i)$ caused by $\Delta Q(t_i)=q(t_i)\Delta t$, the heat equation, the boundary condition and initial condition are needed. There is only transient heat $\Delta Q(t_i)=q(t_i)\Delta t$ at time t_i and no other heat after time t_i, so the right hand of Eq. (1) is zero in this case. (Note that: to use the same expressions of heat equation and boundary condition, $\theta_i(x,t|t_i)$ here should replace $\theta(x,t)$ in the heat equation and the boundary equation given above). For the initial condition at time t_i, $\Delta Q(t_i)$ causes transient temperature variation near position $m=m(t_i)$ and this transient temperature variation can be seen as the initial condition at time t_i, which will be given explicitly in the following sections for three kinds of heat source respectively.

2.1. Single moving heat source

Due to stress concentration caused by the grips of the test machine during experiments, the first phase front can be easily formed at the specimen ends. The schematic diagram of a single moving phase front is shown in Fig. 1. Since experiments were performed in a testing machine at a constant loading rate, the speed of all moving phase fronts (Shaw and Kyriakides, 1995, 1997) was nearly the same according to the kinematical relation $v_N=\dot{\delta}/(N\cdot\varepsilon_T)$, where $\dot{\delta}$ is the elongation rate, N is the number of moving phase fronts, and ε_T is the transformation strain.

The single moving phase front in one-dimensional specimen is treated as a moving point heat source. The release rate of latent heat at the single moving phase front is $q_1=lAv_1=lA\dot{\delta}/\varepsilon_T$, where l is the released latent heat per unit volume and A is the cross-sectional area, and then the transient point heat source derived from the single moving heat source at position $m=m(t_i)$ is

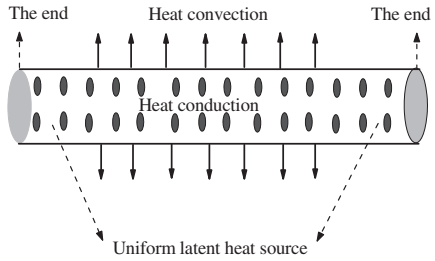

Fig. 4. Schematic diagram of uniform latent heat source in one-dimentional NiTi wire.

$\Delta Q(t_i) = q_1 \Delta t = lA\dot{\delta}\Delta t/\varepsilon_T$. In a very narrow range $[m(t_i) - \beta, m(t_i) + \beta]$, $\beta \to 0$, the transient temperature variation caused by $\Delta Q(t_i)$ is nearly uniform and equals $\theta_{M1} = \Delta Q(t_i)/(2\beta AC_V) = l\dot{\delta}\Delta t/(2\beta C_V \varepsilon_T)$ (see Fig. 2). Hence the initial condition resulted from a single moving heat source at time $t = t_i$ is

$$\theta_i(x, t_i|t_i) = \begin{cases} \theta_{M1} & |x - m(t_i)| \leqslant \beta \\ 0 & |x - m(t_i)| > \beta \end{cases} \tag{4}$$

With the single phase front moving from left to right in the specimen at a constant speed v_1, the heat source position $m(t_i)$ in Eq. (4) is $v_1 t_i$. $\theta_i(x, t|t_i)$ can be obtained by combining heat equation and boundary equation as well as the initial condition Eq. (4). By calculating the limit $\theta(x,t) = \lim_{\mathbf{M}\to\infty} \sum_{i=1}^{\mathbf{M}} \theta_i(x, t|t_i) = \lim_{\mathbf{M}\to\infty} \sum_{i=1}^{\mathbf{M}} G(x, t|t_i)\Delta t = \int_0^t G(x, t|\tau)d\tau$, we can get $\theta(x,t)$ at last. The detailed results are listed in Table 1.

2.2. Two moving heat sources

Similar to the case of a single moving phase front, the stress concentrations commonly result in two fronts emanating nearly simultaneously at the specimen ends (Iadicola and Shaw, 2002; Churchill et al., 2009). Without additional nucleations form, the two fronts (point heat sources), one from the left and the other from the right, move approximately at the same speed v_2 and then

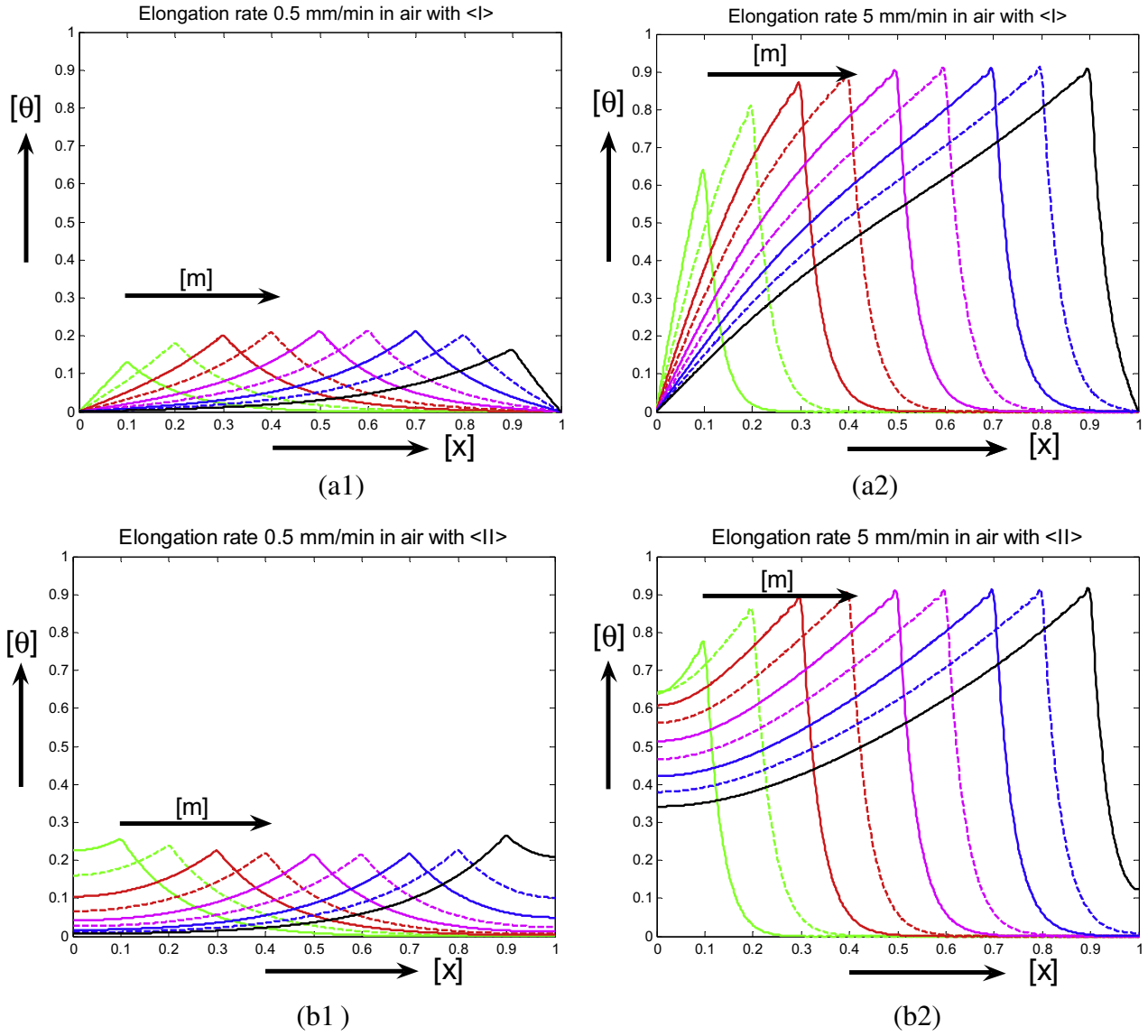

Fig. 5. Temperature profiles for analysis of a single moving phase front, corresponding to three boundary conditions: (a1),(a2) ⟨I⟩; (b1),(b2) ⟨II⟩; (c1),(c2) ⟨III⟩; (d1),(d2) comparisons.

converge in the middle of the specimen. The schematic diagram is shown in Fig. 3.

Similar to Eq. (4), the additional initial condition resulted from the two symmetrical transient heat sources at time $t = t_i$ is

$$\theta_i(x, t_i|t_i) = \begin{cases} \theta_{M2} & |x - m(t_i)| \leqslant \beta \text{ or } |x - (L - m(t_i))| \leqslant \beta \\ 0 & \text{others} \end{cases} \quad (5)$$

where $\theta_{M2} = l\dot{\delta}\Delta t/(4\beta C_V \varepsilon_T)$ $\frac{-b\pm\sqrt{b^2-4ac}}{2a}$, $\beta \to 0$, and $m(t_i) = v_2 t_i$. Note that v_2 is only half of the speed v_1 of a single moving heat source

$\theta_i(x, t|t_i)$

is obtained by combining heat equation and boundary equation as well as the initial condition Eq. (5). And $\theta(x, t)$ is the sum of all the $\theta_i(x, t|t_i)$ in the time range $[0, t]$. The detailed results are listed in Table 1.

2.3. Uniform heat source

In contrast to moving heat sources, this Section discusses the limiting case where volumetric heating occurs uniformly within the specimen at a constant rate. It is true that homogeneous deformation can occur in other SMAs (such as CuAlZn) subjected to more complex stress states and in NiTi under uniaxial compression. Furthermore, at sufficiently high loading rates, numerous nucleations simultaneously occur along the length of NiTi SMAs (Zhang et al., 2010; Sun et al., 2012) and latent heat source is approximately taken as uniform (see Fig. 4).

Interestingly, the temperature variation caused by uniform heat source can also be obtained by using the idea of the additional initial condition used in the moving heat source method. Unlike the position $m(t_i)$ of transient point heat source $\Delta Q(t_i)$ introduced in the case of moving heat sources, however, the transient heat source ΔQ derived from the uniform heat source at time t_i is uniform in the whole length L due to the assumption of homogeneous deformation. The constant release rate q_U of the uniform heat source in length L is $lA\dot{\delta}/\varepsilon_T$, and we have $\Delta Q = q_U \Delta t = lA\dot{\delta}\Delta t/\varepsilon_T$. The temperature variation caused by ΔQ is uniform in L and equals θ_U and then ΔQ can be written as $LAC_V\theta_U$. Hence the additional initial condition resulted from the uniform heat source at time t_i is

$$\theta_i(x, t_i|t_i) = \theta_U, 0 \leqslant x \leqslant L \quad (6)$$

where $\theta_U = l\dot{\delta}\Delta t/(LC_V\varepsilon_T)$.

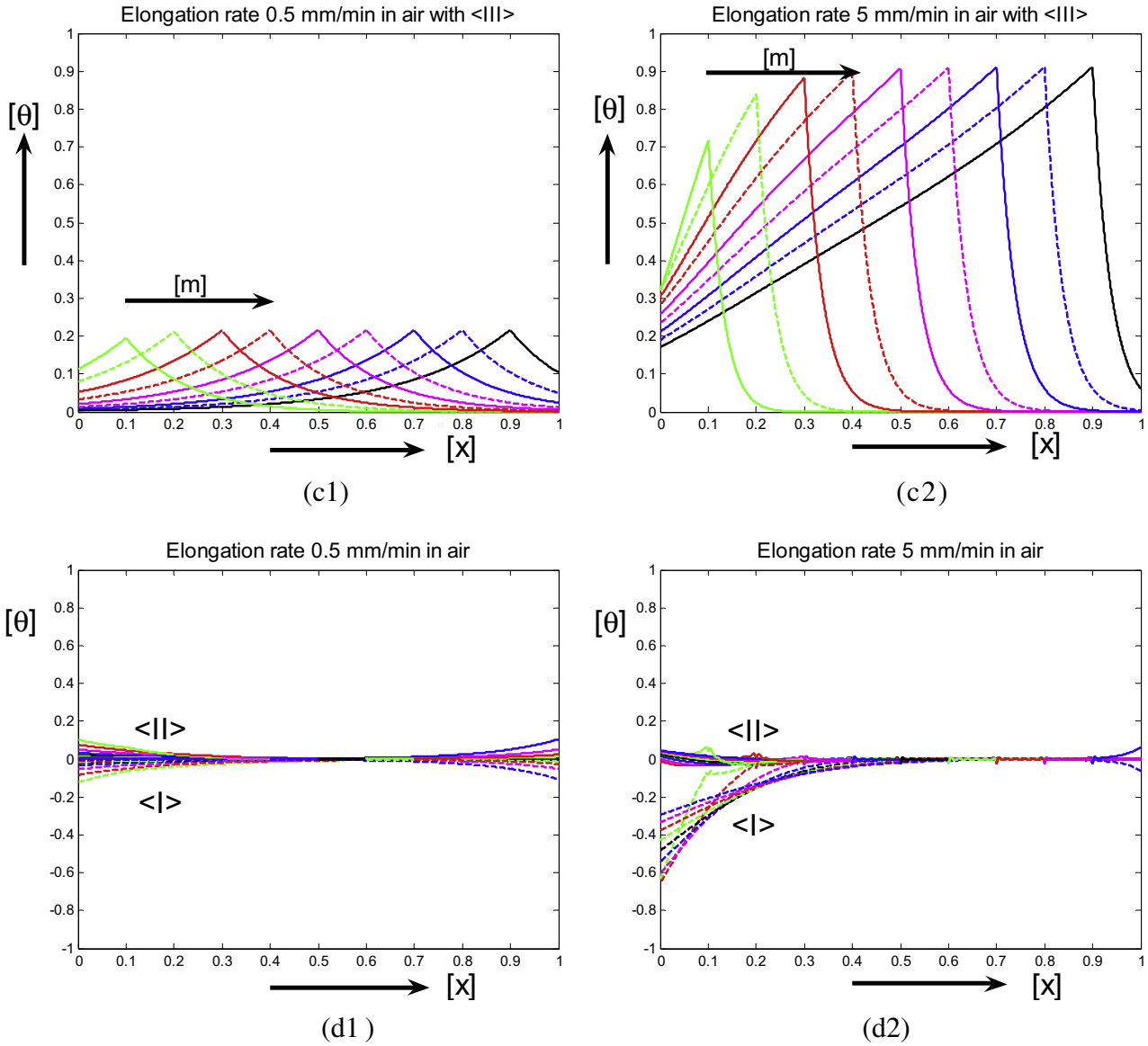

Fig. 5 (*continued*)

$\theta_i(x,t|t_i)$

is obtained by combining heat equation and boundary equation as well as the initial condition Eq. (6). Sum all the $\theta_i(x,t|t_i)$ up in the time range $[0,t]$, we can finally get $\theta(x,t)$. The detailed results can be found in Table 1.

3. Comparisons of temperature variations with three different boundary conditions

Based on the theoretical analysis in Section 2, this Section compares the temperature variations of a NiTi SMA wire with two different elongation rates and three different boundary conditions during the forward phase transformation. The fundamental length scale is the wire length L and the time scale is the duration of the transformation front traversal t_T (which, under steady state conditions, is $L\varepsilon_T/\dot{\delta}$ for a transformation strain of ε_T and elongation rate $\dot{\delta}$, and is also called the transformation time). Here the non-dimensional expressions for axial position, heat source (moving phase front) position, time and temperature variation are defined as $[x] = x/L$, $[m] = m(t)/L$, $[t] = t/t_T$ and $[\theta] = \theta/\theta_0$, respectively; where $\theta_0 = l/C_V$ is the adiabatic temperature rise. The material parameters are listed in Table 2.

Temperature variations $[\theta]$ caused by a single moving heat source with the first, second and 'third' boundary conditions are plotted in Fig. 5(a)–(c), respectively. In each Fig. 9 groups of axial temperature variations are shown corresponding to the increments of moving heat source position ($[m] = 0.1, 0.2, 0.3, \ldots, 0.9$) from left to right in the specimen. At the low elongation rate of 0.5 mm/min, the temperature profiles evolve in a nearly symmetric fashion. At the high elongation rate of 5 mm/min, the temperature evolution becomes skewed and the maximum temperature profiles approach the adiabatic temperature rise $\theta_0 = l/C_V$. Comparisons of $[\theta]$ obtained with three different boundary conditions are given in Fig. 5(d). The detailed comparisons are given by using $[\theta]$ obtained with the first and second boundary conditions minus $[\theta]$ obtained with the 'third' boundary condition, respectively. It is shown that $[\theta]$ with the second boundary condition ⟨II⟩ is larger while $[\theta]$ with the first boundary condition ⟨I⟩ is smaller than $[\theta]$ with the 'third' boundary condition ⟨III⟩. Especially, the differences are very

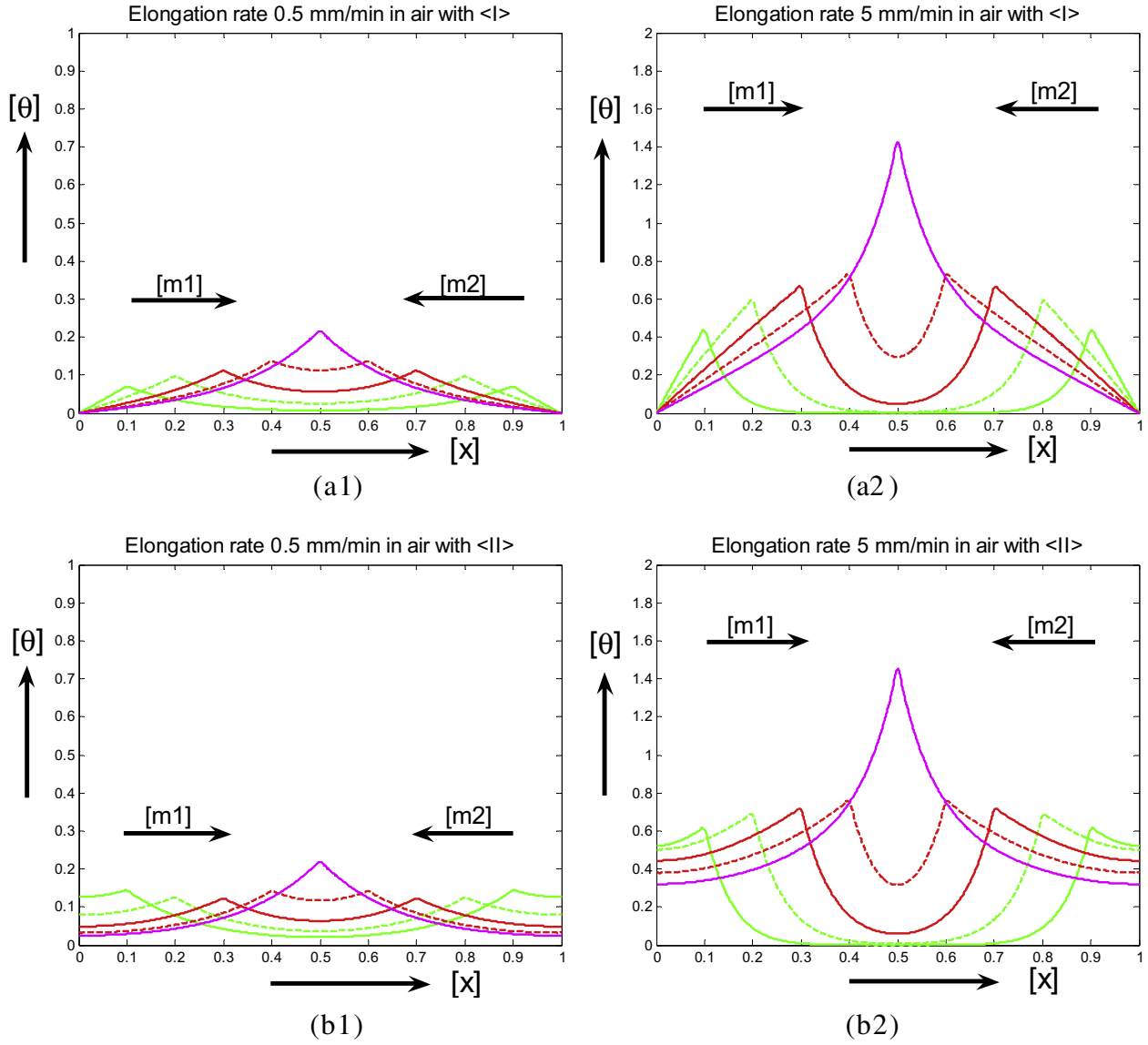

Fig. 6. Temperature profiles for analysis of two moving phase fronts, corresponding to three boundary conditions: (a1),(a2) ⟨I⟩; (b1),(b2) ⟨II⟩; (c1),(c2) ⟨III⟩; (d1),(d2) comparisons.

obvious near the specimen ends at high elongation rates. Note that the phase transformation via a single front is only possible at relatively low loading rates, or is at best short-lived at faster rates (Shaw and Kyriakides, 1997; Iadicola and Shaw, 2004). This is because the higher the loading rate, the faster the release of latent heat, and the larger peak temperature on moving phase front and therefore a larger temperature dependent transformation stress is needed. Large stress leads to additional fronts in the specimen. The issue is discussed in Section 4.1.

Temperature variations $[\theta]$ caused by two moving heat sources with the first, second and 'third' boundary conditions are plotted in Fig. 6(a)–(c), respectively. One moves from the left to the middle, corresponding to the increments of moving heat source position $[m1]$=0.1, 0.2, 0.3, 0.4, 0.5, while the other moves from the right to middle, corresponding to the decrements of moving heat source position $[m2]$ = 0.9, 0.8, 0.7, 0.6, 0.5. The numerical simulations clearly show that the temperature profile becomes larger when the two moving fronts are close to each other. Finally, the maximum temperature, which exceeds the adiabatic temperature rise $\theta_0 = l/C_V$ by as much as a factor of two, is obtained at $[m1] = [m2] = 0.5$ where the two converging phase fronts coalesce. This interesting temperature profile has been observed by many experiments (Shaw and Kyriakides, 1995, 1997; He et al., 2010; Zhang et al., 2010). Similar to the case of a single phase front, the effects of boundary conditions on temperature variations are significant near the specimen ends, but can be neglected in the middle (see the comparisons plotted in Fig. 6(d)).

Temperature variations $[\theta]$ caused by uniform heat source with the first, second and 'third' boundary conditions are shown in Fig. 7. In each Fig. 9 groups of axial temperature variations are shown corresponding to the increments of time ($[t] = 0.1, 0.2, 0.3, \ldots, 0.9$) during the forward phase transformation. Similar to the cases of moving heat sources, the boundary effects on temperature variations can also be found in this case of uniform heat source.

The above analyses show that different boundary conditions lead to different temperature profiles in one-dimensional NiTi SMAs, and these differences are significant at the specimen ends. In practice, the accurate description of boundary effects is difficult. For example, the dog-bone shape of some specimens (strips or sheets) and contact conditions (for example, thermal resistance) between the specimen ends and the grips of test machine make

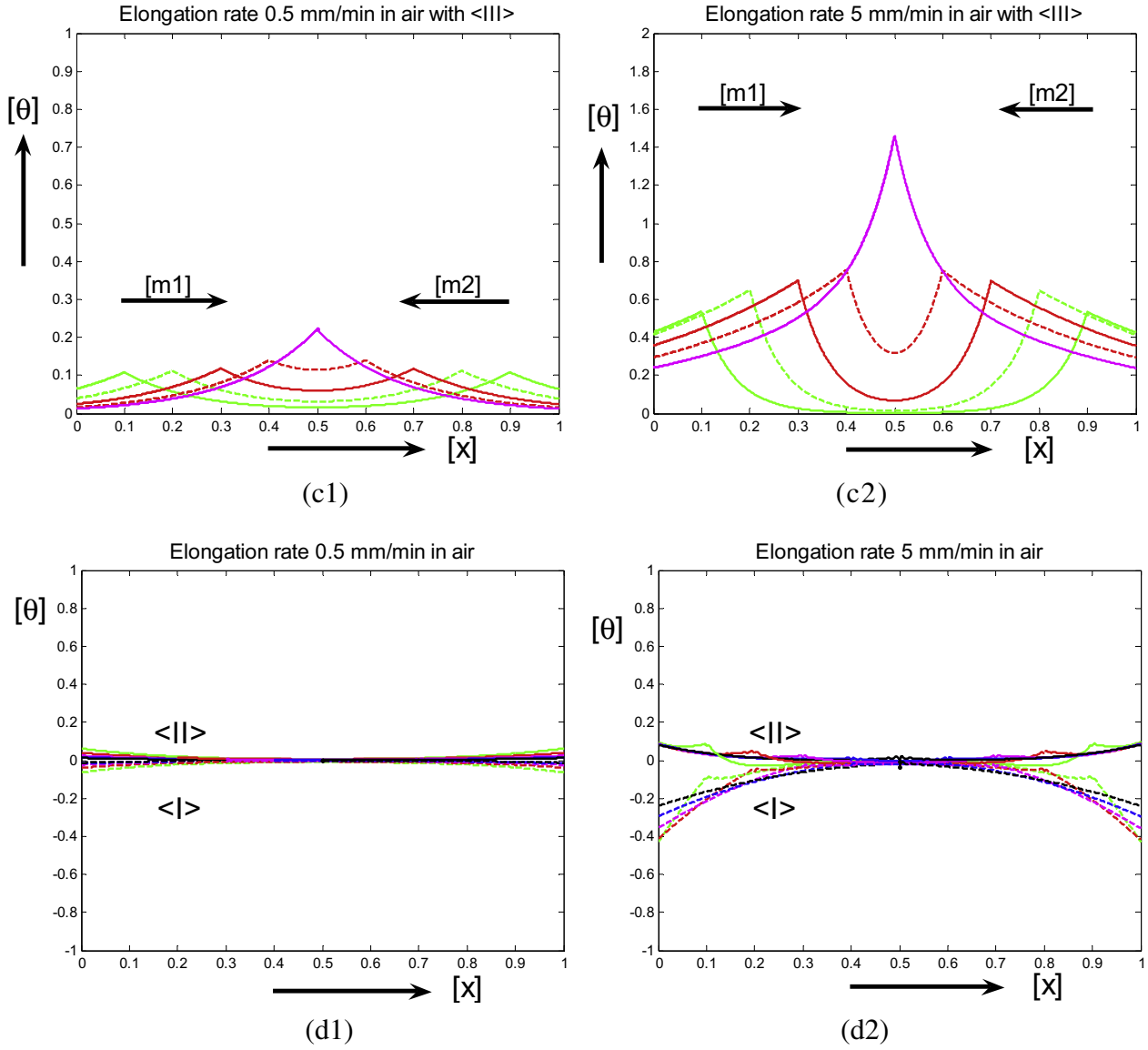

Fig. 6 (*continued*)

heat exchange very complicated at the boundary. Therefore, the appropriate simplifications of boundary conditions in Section 2 are usually used in the modeling of thermo-mechanical behavior of SMAs.

4. Discussion of rate-dependent phenomena

4.1. Nucleation of new phase fronts

Superelastic fine-grained NiTi polycrystalline SMAs under tensile loading deform collectively via the nucleation and movement of macroscopic phase fronts. Experiments (Leo et al., 1993; Shaw and Kyriakides, 1995, 1997; Zhang et al., 2010) showed that the number of phase fronts increases with increasing loading rate. In detail, nucleation of martensite in an austenitic region is a distinct event requiring a higher nucleation stress σ_N than the propagation stress σ_P required subsequently to continue the forward transformation (see Fig. 8(a)). From the existing theories and experiments (Shaw and Kyriakides, 1995, 1997; Vitiello et al., 2005; Churchill et al., 2009; Sun et al., 2012), temperature dependent σ_N and σ_P can be approximated by linear functions of temperature (see Fig. 8(b)). The difference $\Delta\sigma$ between σ_N and σ_P, coupled with the local temperature change caused by the latent heat source, governs the number of nucleations of phase fronts.

We start with a single phase front moving from left to right in a specimen with a constant speed v_1 (Section 2.1). When the single phase front moves to position m at time t, where $t = m/v_1$, the phase front temperature (peak temperature) is $\theta_{front} = \theta(m, m/v_1)$. Take the peak temperature obtained with the 'third' boundary condition as an example, substituting $t = m/v_1$ into $\langle S\rangle + \langle III\rangle + \langle\theta\rangle$ listed in Table 1 leads to

$$\theta_{front}\left(m, \frac{m}{v_1}\right) = \frac{lv_1}{\sqrt{(C_V v_1)^2 + 4Phk/A}} erf\left(\sqrt{\left(\frac{Ph}{AC_V} + \frac{C_V v_1^2}{4k}\right)}\frac{m}{v_1}\right) \tag{7}$$

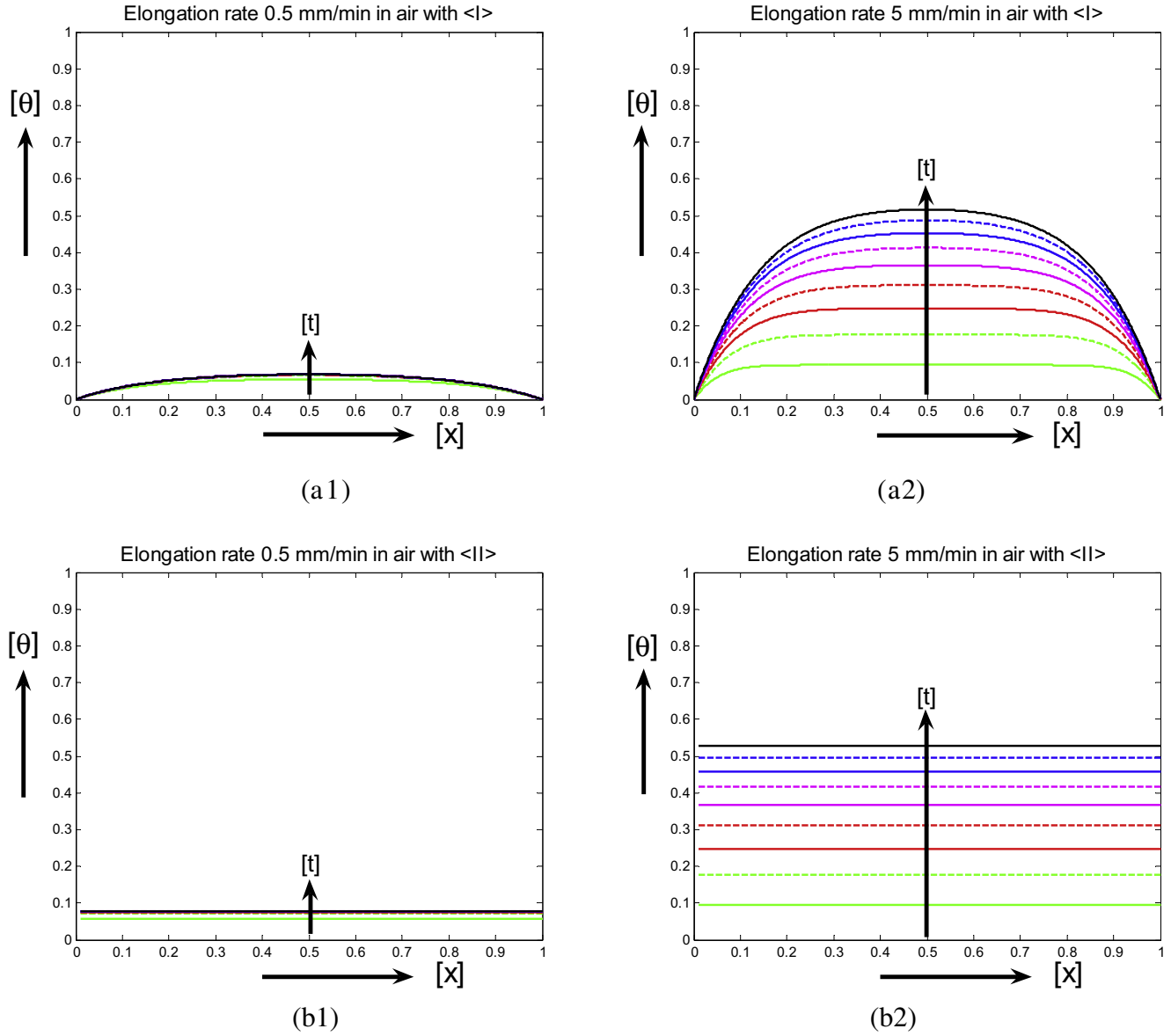

Fig. 7. Temperature profiles for analysis of uniform latent heat source, corresponding to three boundary conditions: (a1),(a2) ⟨I⟩; (b1),(b2) ⟨II⟩; (c1),(c2) ⟨III⟩; (d1),(d2) comparisons.

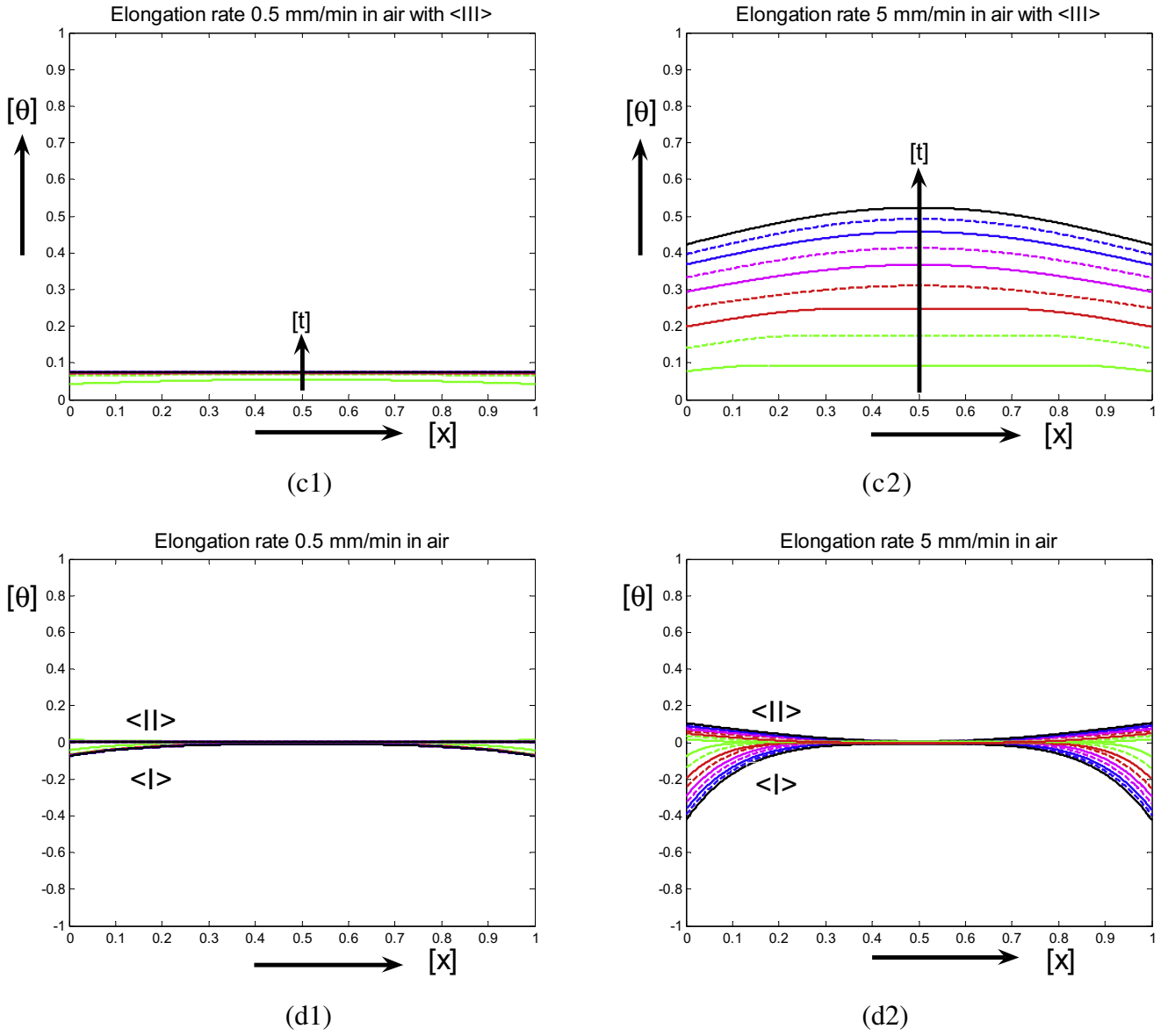

Fig. 7 (*continued*)

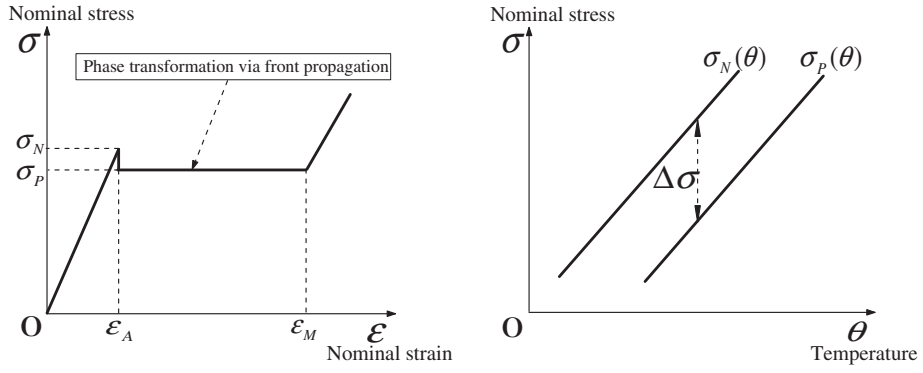

Fig. 8. (a) Schematic stress–strain curve in the quasi-static loading process; (b) temperature dependent nucleation stress and front propagation stress.

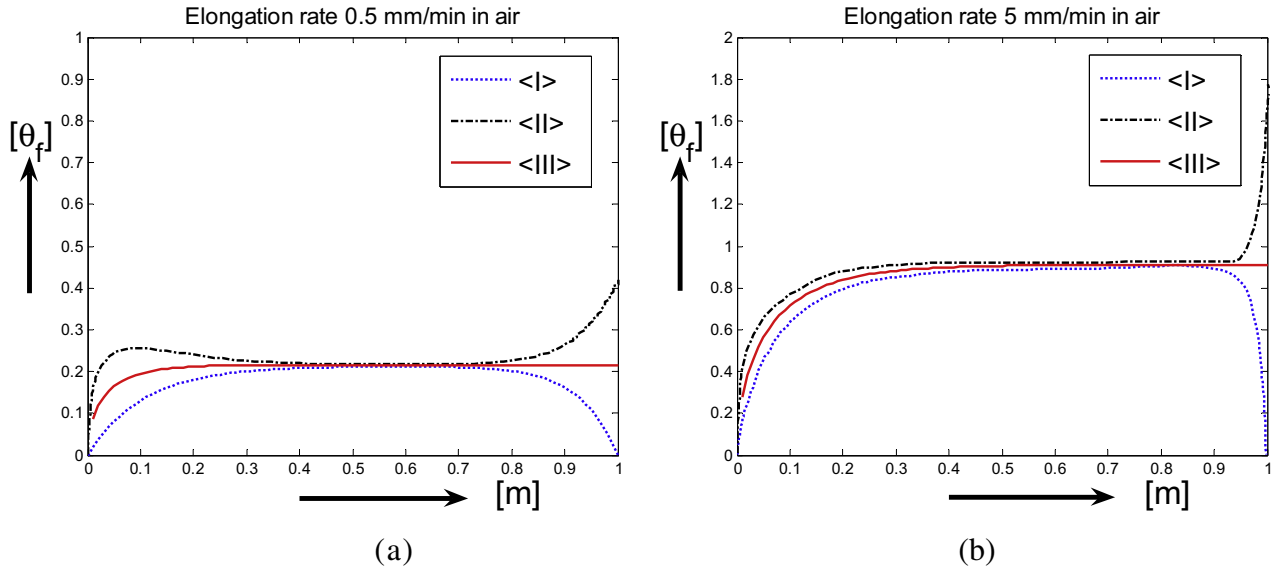

Fig. 9. Peak temperature evolution for a single moving phase front, corresponding to two elongation rates in air: (a) 0.5 mm/min, (b) 5 mm/min.

where $erf(\eta) = \frac{2}{\sqrt{\pi}} \int_0^\eta e^{-\varsigma^2} d\varsigma$ is the error function.

If the time $t = m/v_1 \to \infty$, the error function $erf\left(\sqrt{\left(\frac{Ph}{AC_V} + \frac{C_V v_1^2}{4k}\right)\frac{m}{v_1}}\right) \to 1$, and Eq. (7) reduces to $\theta_{front} = lv_1/\sqrt{(C_V v_1)^2 + 4Phk/A}$, which is the classical closed-form expression of the relation between the temperature increase and the speed of the interface (Bruno et al., 1995).

Fig. 9 shows the evolution of $[\theta_f] = \theta_{front}/\theta_0$ with three different boundary conditions. The differences of the three lines are not significant except at the specimen right end, where $[\theta_f]$ immediately decreases to zero with the boundary condition ⟨I⟩ while it increases steeply with the boundary condition ⟨II⟩. At a very low loading rate, the behavior is nearly isothermal. At a higher loading rate, the local σ_P increases with the increasing θ_{front} (see Fig. 8(b)). As long as the local value of $\sigma_P = \sigma_P(\theta_{front})$ remains less than $\sigma_N = \sigma_N(\theta)$ in the cooler untransformed region, the front continues to propagate at a constant speed (Shaw and Kyriakides, 1997). As we saw in Fig. 9(b), if the loading rate is high enough so that the internal heat does not have enough time to dissipate and the front temperature keeps rising, the value of $\sigma_P = \sigma_P(\theta_{front})$ will eventually exceed $\sigma_N = \sigma_N(\theta)$ of some other colder, untransformed region, enabling the nucleation of new phase fronts at a second site. Since the single phase front is moving from left to right, the coolest point in the untransformed region is at the specimen right end. The difference between the temperature of the moving phase front and the temperature of the specimen right end should be given to get the effects of axial temperature variation on the nucleation of new phase front at the right end. Regardless of the temperature variation at the specimen end, many experiments (Shaw and Kyriakides, 1995, 1997; Chang et al., 2006; Churchill et al., 2009; Zhang et al., 2010; Sun et al., 2012) showed that new phase fronts were usually formed at the specimen ends due to the stress concentration caused by the grip of test machine. If the loading rate continues to increase, numerous phase fronts will be formed successively. Based on the above discussion, we have seen that the front speed, the front temperature and the propagation stress are coupled. The coexistence of more than one front is the product of a sequence of events as described above. According to the above scenario of thermo-mechanical coupling, models and computational studies were performed (Shaw, 2000; Iadicola and Shaw, 2004; He and Sun, 2010; Sun et al., 2012) and important insight into the multiple-front formations has been obtained.

4.2. Rate-dependent stress hysteresis (or damping capacity)

For the stress–strain curve of SMAs, the stress hysteresis is the value between the forward and reverse phase transformation plateaus, which directly determines the damping capacity. Some experiments (Leo et al., 1993; Tobushi et al., 1998; Pieczyska et al., 2005) showed an increase in hysteresis with increasing rate while others (Gandhi and Wolons, 1999; Dolce et al., 2000; Heller et al., 2009) showed a decrease in hysteresis with increasing rate. More recent experiments (Piedboeuf et al., 1998; Vitiello et al., 2005; Zhu and Zhang, 2007; Dayananda and Subba Rao, 2008; He et al., 2010; Zhang et al., 2010) showed that the rate dependence of hysteresis is non-monotonic with a hysteresis peak at an intermediate loading rate that depends on the ambient condition and the geometry of the specimen.

These rate-dependent mechanical behaviors involve the coupling between the temperature dependence of transformation stress, latent heat and heat exchange with the ambient conditions. Therefore, the temperature analyses in Section 2 are useful to understand the sensitivity of the thermal behavior to the mechanical behavior of SMAs. For example, the evolution of the temperature of the specimen used in the theoretical models (Entemeyer et al., 2000; Vitiello et al., 2005; Zhu and Zhang, 2007; He and Sun, 2011) for rate-dependent mechanical responses of SMAs is the case of ⟨U⟩ + ⟨II⟩ + ⟨θ⟩ listed in Table 1.

5. Conclusions

This paper studies the temperature variations in one-dimensional superelastic NiTi SMAs under different loading rates and boundary conditions during the stress-induced forward transformation. The local heating of the phase front causes a rise in the local temperature, which in turn results in a vertical shift of the local stress–strain response due to the material's inherent sensitivity to temperature. For the case of localized deformation, the moving phase fronts are treated as moving point heat sources; for the case of homogeneous deformation (an infinite number of fronts), a uniform latent heat source is assumed in the specimen. Temperature variations in both cases are solved by the moving heat source method based on the heat diffusion equation. Especially, the closed-form expression, a relation between the temperature increase and the speed of the phase interface, proposed by Bruno

et al. (1995) in the form of a traveling wave in an infinitely long wire is only a special case of $\langle S\rangle + \langle III\rangle + \langle\theta\rangle$, $t \to \infty$, listed in Table 1. The temperature variation of a NiTi SMA wire under Dirichlet condition with moving point heat sources solved by using the Dirac delta function (Iadicola and Shaw, 2004) is also presented in this paper by using the moving heat source method. In addition, the temperature evolution of one-dimensional NiTi SMAs with the second (Neumann condition) and 'third' boundary conditions are also solved. Comparisons of temperature variations with three different boundary conditions clearly show that the effects of boundary conditions on temperature variations are significant near the specimen ends, but negligible in the middle.

Acknowledgments

The authors acknowledge the financial support of National Natural Science Foundation of China (No. 11132003, 11172033, 10972027, 11272044 and 11272136) and National Basic Research Program of China (973 Program) (2010CB7321004).

References

Abeyaratne, R., Knowles, J.K., 1993. A continuum model of a thermoelastic solid capable of undergoing phase transitions. J. Mech. Phys. Solids 41, 541–571.
Auricchio, F., Sacco, E., 2001. Thermo-mechanical modelling of a superelastic shape-memory wire under cyclic stretching-bending loadings. Int. J. Solids Struct. 38, 6123–6145.
Balandraud, X., Chrysochoos, A., Leclercq, S., Peyroux, R., 2001. Influence of the thermomechanical coupling on the propagation of a phase change front. C. R. Acad. Sci. Ser. IIb Mec. 329, 621–626.
Bhattacharya, K., 2003. Microstructure of Martensite: Why It Forms and How It Gives Rise to the Shape-Memory Effect. Oxford University Press.
Brinson, L.C., Schmidt, I., Lammering, R., 2004. Stress-induced transformation behavior of a polycrystalline NiTi shape memory alloy: micro and macromechanical investigations via in situ optical microscopy. J. Mech. Phys. Solids 52, 1549–1571.
Bruno, O.P., Leo, P.H., Reitich, F., 1995. Free boundary conditions at austenite-martensite interfaces. Phys. Rev. Lett. 74, 746–749.
Chang, B.C., Shaw, J.A., Iadicola, M.A., 2006. Thermodynamics of shape memory alloy wire: modeling, experiments, and application. Con. Mech. Thermodyn. 18, 83–118.
Chrysochoos, A., Licht, C., Peyroux, R., 2003. A one-dimensional thermomechanical modeling of phase change front propagation in a SMA monocrystal. C. R. Mecanique 331, 25–32.
Churchill, C.B., Shaw, J.A., Iadicola, M.A., 2009. Tips and tricks for characterizing shape memory alloy wire: Part 3 - Localization and propagation phenomena. Exp. Tech. 33, 70–78.
Dayananda, G.N., Subba Rao, M., 2008. Effect of strain rate on properties of superelastic NiTi thin wires. Mater. Sci. Eng. A 486, 96–103.
Dolce, M., Cardone, D., Marnetto, R., 2000. Implementation and testing of passive control devices based on shape memory alloys. Earthquake Eng. Struct. Dyn. 29, 945–968.
Entemeyer, D., Patoor, E., Eberhardt, A., Berveiller, M., 2000. Strain rate sensitivity in superelasticity. Int. J. Plast. 16, 1269–1288.
Favier, D., Louche, H., Schlosser, P., Orgéas, L., Vacher, P., Debove, L., 2007. Homogeneous and heterogeneous deformation mechanisms in an austenitic polycrystalline Ti-50.8 at.% Ni thin tube under tension. Investigation via temperature and strain fields measurements. Acta Mater. 55, 5310–5322.
Feng, P., Sun, Q.P., 2006. Experimental investigation on macroscopic domain formation and evolution in polycrystalline NiTi microtubing under mechanical force. J. Mech. Phys. Solids 54, 1568–1603.
Gandhi, F., Wolons, D., 1999. Characterization of the pseudoelastic damping behavior of shape memory alloy wires using complex modulus. Smart Mater. Struct. 8, 49–56.
Grabe, C., Bruhns, O.T., 2008. On the viscous and strain rate dependent behavior of polycrystalline NiTi. Int. J. Solids Struct. 45, 1876–1895.
Grandi, D., Maraldi, M., Molari, L., 2012. A macroscale phase-field model for shape memory alloys with non-isothermal effects: influence of strain rate and environmental conditions on the mechanical response. Acta Mater. 60, 179–191.
He, Y.J., Sun, Q.P., 2010. Rate-dependent domain spacing in a stretched NiTi strip. Int. J. Solids Struct. 47, 2775–2783.
He, Y.J., Sun, Q.P., 2011. On non-monotonic rate dependence of stress hysteresis of superelastic shape memory alloy bars. Int. J. Solids Struct. 48, 1688–1695.
He, Y.J., Yin, H., Zhou, R.H., Sun, Q.P., 2010. Ambient effects on damping peak of shape memory alloy. Mater. Lett. 64, 1483–1486.
Heller, L., Sittner, P., Pilch, J., Landa, M., 2009. Factors controlling superelastic damping capacity of SMAs. J. Mater. Eng. Perform. 18, 603–611.
Iadicola, M.A., Shaw, J.A., 2002. An experimental setup for measuring unstable thermo-mechanical behavior of shape memory alloy wire. J. Intell. Mater. Syst. Struct. 13, 157–166.
Iadicola, M.A., Shaw, J.A., 2004. Rate and thermal sensitivities of unstable transformation behavior in a shape memory alloy. Int. J. Plast. 20, 577–605.
Leclercq, S., Lexcellent, C., 1996. A general macroscopic description of the thermomechanical behavior of shape memory alloys. J. Mech. Phys. Solids 44, 953–980.
Leo, P.H., Shield, T.W., Bruno, O.P., 1993. Transient heat transfer effects on the pseudoelastic behavior of shape-memory wires. Acta Metall. Mater. 41, 2477–2485.
Lim, T.J., McDowell, D.L., 2002. Cyclic thermomechanical behavior of a polycrystalline pseudoelastic shape memory alloy. J. Mech. Phys. Solids 50, 651–676.
Morin, C., Moumni, Z., Zaki, W., 2011. A constitutive model for shape memory alloys accounting for thermomechanical coupling. Int. J. Plast. 27, 748–767.
Otsuka, K., Wayman, C.M., 1998. Shape Memory Materials. Cambridge University Press.
Pieczyska, E., Gadaj, S., Nowacki, W.K., Hoshio, K., Makino, Y., Tobushi, H., 2005. Characteristics of energy storage and dissipation in TiNi shape memory alloy. Sci. Technol. Adv. Mater. 6, 889–894.
Piedboeuf, M.C., Gauvin, R., Thomas, M., 1998. Damping behaviour of shape memory alloys: strain amplitude, frequency and temperature effects. J. Sound Vib. 214 (5), 885–901.
Puglisi, G., Truskinovsky, L., 2005. Thermodynamics of rate-independent plasticity. J. Mech. Phys. Solids 53, 655–679.
Shaw, J.A., 2000. Simulations of localized thermo-mechanical behavior in a NiTi shape memory alloy. Int. J. Plast. 16, 541–562.
Shaw, J.A., Kyriakides, S., 1995. Thermomechanical aspects of NiTi. J. Mech. Phys. Solids 43, 1243–1281.
Shaw, J.A., Kyriakides, S., 1997. On the nucleation and propagation of phase transformation fronts in a NiTi alloy. Acta Mater. 45, 683–700.
Sun, Q.P., He, Y.J., 2008. A multiscale continuum model of the grain-size dependence of the stress hysteresis in shape memory alloy polycrystals. Int. J. Solids Struct. 45, 3868–3896.
Sun, Q.P., Li, Z.Q., 2002. Phase transformation in superelastic NiTi polycrystalline micro-tubes under tension and torsion-from localization to homogeneous deformation. Int. J. Solids Struct. 39, 3797–3809.
Sun, Q.P., Zhao, H., Zhou, R., Saletti, D., Yin, H., 2012. Recent advances in spatiotemporal evolution of thermomechanical fields during the solid-solid phase transition. C. R. Mecanique 340, 349–358.
Tobushi, H., Shimeno, Y., Hachisuka, T., Tanaka, K., 1998. Influence of strain rate on superelastic properties of TiNi shape memory alloy. Mech. Mater. 30, 141–150.
Vitiello, A., Giorleo, G., Morace, R.E., 2005. Analysis of thermomechanical behaviors of Nitinol wires with high strain rates. Smart Mater. Struct. 14, 215–221.
Zhang, X.H., Feng, P., He, Y.J., Yu, T.X., Sun, Q.P., 2010. Experimental study on rate dependence of macroscopic domain and stress hysteresis in NiTi shape memory alloy strips. Int. J. Mech. Sci. 52, 1660–1670.
Zhu, S., Zhang, Y., 2007. A thermomechanical constitutive model for superelastic SMA wire with strain-rate dependence. Smart Mater. Struct. 16, 1696–1707.